

The coronal line regions of planetary nebulae NGC 6302 and 6537: 3–13 μm grating and echelle spectroscopy

S. Casassus,¹ P. F. Roche^{1*} and M. J. Barlow²

¹*Astrophysics, Nuclear and Astrophysics Laboratory, Physics Department, Oxford University, Keble Road, Oxford OX1 3RH*

²*Department of Physics and Astronomy, University College London, Gower Street, London WC1E 6BT*

Accepted 1999 November 3. Received 1999 August 9; in original form 1999 January 19

ABSTRACT

We report on advances in the study of the cores of NGC 6302 and 6537 using infrared grating and echelle spectroscopy. In NGC 6302, emission lines from species spanning a large range of ionization potential, and in particular [Si IX] 3.934 μm , are interpreted using photoionization models (including CLOUDY), which allow us to re-estimate the temperature of the central star to be about 250 000 K. All of the detected lines are consistent with this value, except for [Al V] and [Al VI]. Aluminium is found to be depleted to one hundredth of the solar abundance, which provides further evidence for some dust being mixed with the highly ionized gas (with photons harder than 154 eV). A similar depletion pattern is observed in NGC 6537. Echelle spectroscopy of IR coronal ions in NGC 6302 reveals a stratified structure in ionization potential, which confirms photoionization to be the dominant ionization mechanism. The lines are narrow ($<22 \text{ km s}^{-1}$ FWHM), with no evidence of the broad wings found in optical lines from species with similar ionization potentials, such as [Ne V] 3426 Å. We note the absence of a hot bubble, or a wind-blown bipolar cavity filled with a hot plasma, at least on 1 arcsec and 10 km s^{-1} scales. The systemic heliocentric velocities for NGC 6302 and 6537, measured from the echelle spectra of IR recombination lines, are found to be $-34.8 \pm 1 \text{ km s}^{-1}$ and $-17.8 \pm 3 \text{ km s}^{-1}$. We also provide accurate new wavelengths for several of the infrared coronal lines observed with the echelle.

Key words: ISM: abundances – ISM: kinematics and dynamics – planetary nebulae: individual: NGC 6302 – planetary nebulae: individual: NGC 6537 – infrared: ISM: lines and bands.

1 INTRODUCTION

The extreme high-excitation planetary nebulae (PNe) NGC 6302 and 6537, which are both bipolar and of Peimbert's Type I, show lines from the highest ionization species found in PNe (e.g. [Si VI] 1.96 μm , Ashley & Hyland 1988, hereafter AH88) as well as fast flows of order 1000 km s^{-1} (Meaburn & Walsh 1980). Proposed ionization mechanisms include photoionization by a very hot central star, or shock excitation (e.g. Rowlands, Houck & Herter 1994; Lamé & Ferland 1991; AH88; Barral et al. 1982). Pottasch et al. (1996) published a portion of the *ISO* (*Infrared Space Observatory*) spectrum of NGC 6302, and found that the properties of the spectrum can be well accounted for by photoionization by a 380 000 K greybody central star, using the photoionization code CLOUDY (Ferland 1996).

We report here on a study of the cores of NGC 6302 and 6537 using near- and mid-infrared spectroscopy. Low- and

medium-resolution CGS3 and CGS4 infrared spectra taken at UKIRT have higher sensitivity in the atmospheric windows than the SWS on *ISO*, and our spectrum of NGC 6302 shows the presence of [Si IX] 3.934 μm , which had only been tentatively detected in the *ISO* spectrum. This detection has allowed us to reestimate the temperature of the central star to be about 250 000 K, the upper limit inferred by Marconi et al. (1996) from the non-detection of [Si IX] by Oliva, Pasquali & Reconditi (1996).

We also present unprecedentedly high dispersion infrared echelle spectra of the cores of these nebulae. Knowledge of the physical conditions and velocity fields in the obscured cores of bipolar PNe is the key to constructing models, but these are currently inferred only through extrapolation from optical studies. We show here that tracing the velocity field with coronal ions leads to quite a different picture of the structure of these bipolar planetary nebulae.

The infrared coronal lines are in fact very narrow, with no evidence of the fast flows detected in [Ne V] 3426 Å towards the

* E-mail: pfr@astro.ox.ac.uk

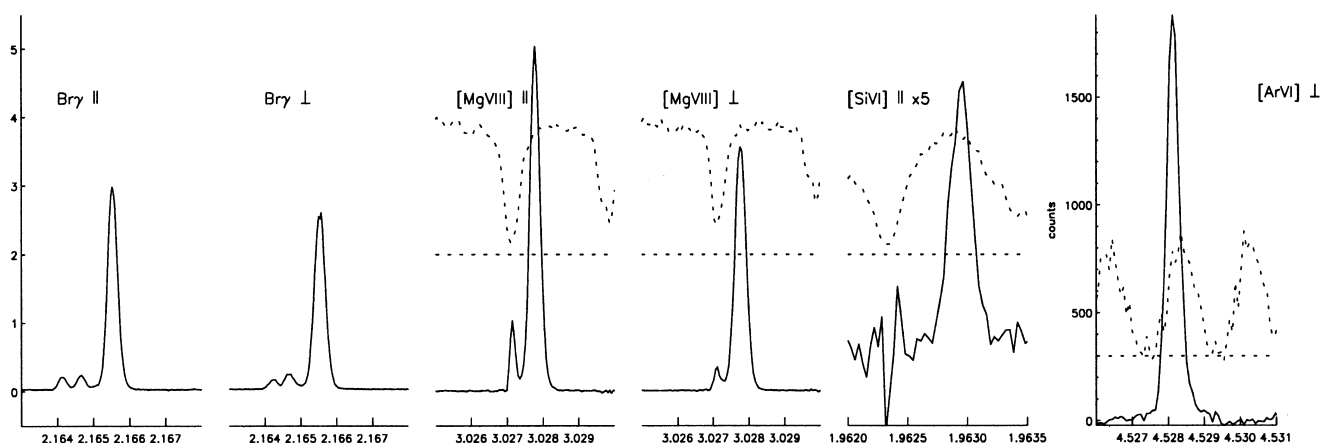


Figure 3. Lines observed from NGC 6302 with the CGS4 echelle. Flux densities are given in $10^{-12} \text{ W m}^{-2} \mu\text{m}$, and the calibrated wavelengths for the rest frame of the nebula are in μm . The dotted lines show the standard star spectra used to flux calibrate the observations, doppler shifted to the rest frame of NGC 6302. The feature in the short wavelength wing of the [Mg VIII] line could not be identified. The dotted curve over the [Ar VI] spectrum corresponds to the CVF fringe pattern. The rms noise level is $5 \times 10^{-15} \text{ W m}^{-2} \mu\text{m}$ in the [Mg VIII] spectra, and 19 counts in the [Ar VI] spectrum.

2.2 Echelle spectroscopy

The nebulae were observed with the CGS4 short camera and echelle at UKIRT on 1997 May 11 and 12. Two out of three nights were clear, so the observations are not as complete as hoped. In the case of NGC 6302, an infrared disc lies at the waist of the bipolar structure, where a dark lane is seen in optical images (Lester & Dinerstein 1984). We oriented the CGS4 slit along two perpendicular position angles, the \parallel position lies at -20° , along the dark lane at the waist of the nebula, and the \perp position lies at -110° , along the bipolar axis. We only obtained echelle spectra with the \parallel position angle for NGC 6537, at -45° . The list of observed lines and their orientation in NGC 6302 is: Bry, \perp & \parallel ; [Mg VIII], \perp & \parallel ; [Si VI], \parallel ; [Ar VI], \perp . In NGC 6537, we observed Bry, [Si VI], and [Ar VI], all at the \parallel slit orientation.

At wavelengths near $4 \mu\text{m}$, the order sorting CVF filter produced interference fringes, hampering the data acquisition. In the case of [Ar VI], the line was close to a fringe maximum, and the spatial distribution could still be determined. This ionic line was one of the best candidates to trace the velocity field because it is one of the very brightest, and also because its ionization potential is only a little less than that of Ne V, in which Meaburn & Walsh (1980) detected 1000 km s^{-1} wide wings. We were not able to obtain echelle measurements of [Si IX] $3.934 \mu\text{m}$, the highest excitation line so far detected from NGC 6302. Transmission modulation by the fringes completely dominates the emission from [Si IX], which is more than a thousand times fainter than the [Ar VI] line.

A resolving power of ~ 20000 can be achieved with the echelle and UKIRT's CGS4 spectrometer, corresponding to a velocity resolution of 15 km s^{-1} . With the short camera and a one-pixel-wide slit, the pixel size is about 1.5 arcsec spatially and 1 arcsec spectrally. We oversampled the spectra by shifting the array three times over two pixels.

Figs 3 and 4 show the spectra obtained by collapsing all the emission along the slit. In the cases where it was relevant (i.e. when there was significant structure), the spectrum of a standard star is superposed in dotted lines on the spectrum of the nebular ion. The standard star spectra are shown in arbitrary units, but zero counts are represented by the horizontal dotted lines. Figs 9 and 10

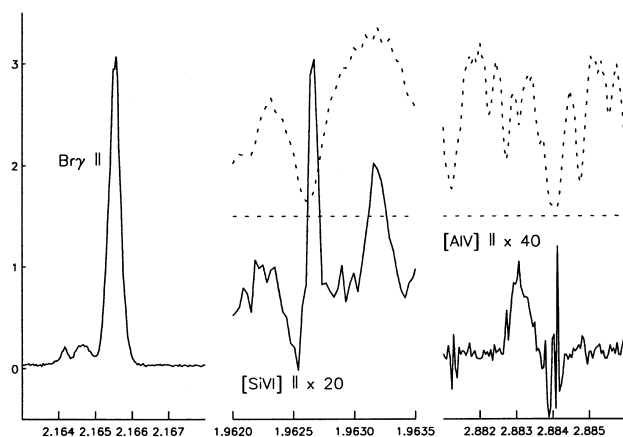


Figure 4. Lines observed from NGC 6537. Flux densities are given in $10^{-12} \text{ W m}^{-2} \mu\text{m}$, and wavelengths are in μm and in the rest frame of the nebula. The dotted lines are the standard star spectra used to flux calibrate the observations, doppler shifted to the rest frame of the NGC 6537.

contain the reduced frames for the lines observed with CGS4 + echelle.

The secondary line at $3.0271 \mu\text{m}$ apparent in the [Mg VIII] spectra for both slit positions could not be identified. It is not believed to be a [Mg VIII] $3.028 \mu\text{m}$ velocity component at -64 km s^{-1} because it is not seen in the spectra of the other ions. Neither is it an atmospheric transmission feature, which can be concluded by inspecting the frames presented in Fig. 9, nor is it a leak from neighbouring orders. It is nonetheless probable that the secondary line originates from a coronal ion formed with an ionization potential between that required to produce Si VI and Si IX (i.e. from 166.77 to 303.16 eV), because the low-resolution spectrum of NGC 6537 shows no sign of any line at all near $3.028 \mu\text{m}$. A Doppler shift of the secondary line deeper into the atmospheric transmission trough seen in Fig. 3 is discarded on the basis that at the time of the echelle observations, the velocity of NGC 6302 was $-49 \pm 1 \text{ km s}^{-1}$, in the Earth's rest frame, whereas at the time of the low-resolution observations, NGC 6537 was at $-42 \pm 3 \text{ km s}^{-1}$ (see Appendix A).

In the Br γ frame (Fig. 3), the fluxes and wavelengths of the two secondary lines correspond to He I 4–7 at 2.16415 μm (the singlet $^1\text{F}^{\circ}-^1\text{G}$ and triplet $^3\text{F}^{\circ}-^3\text{G}$ transitions are blended) and He II 8–14 at 2.16464 μm , using the emissivity tables from Smits (1991) and Hummer & Storey (1987).

Only the raw observation is shown for [Ar VI]. This frame was affected by the CVF fringes, which can be seen in the spectrum of the standard star shown by the dotted line. However, a flux calibration is possible and the total [Ar VI] flux through the one-pixel 1-arcsec-wide slit is about 10 times that for [Mg VIII]. A higher [Ar VI] flux relative to [Mg VIII] is found in the low-resolution spectrum, with a 3-arcsec slit, which is an indication that the [Ar VI] emission has a larger spatial extent than [Mg VIII].

3 ABUNDANCE STUDY AND PHOTOIONIZATION MODELS

3.1 Extinction estimates and emission measures

We shall adopt for NGC 6302 the density and temperature estimated by Oliva et al. (1996) from a variety of transitions, $T_e = 19\,000\text{ K}$ (e.g. from [Ar V] $\lambda\lambda 4626, 7006$ and [Ne IV] $\lambda\lambda 2422, 4725$), and $N_e = 18\,000\text{ cm}^{-3}$. For NGC 6537 we used the [O III] electron temperature $T_e = 16\,000\text{ K}$ and $N_e = 17\,000\text{ cm}^{-3}$ from Feibelman et al. (1985). In the case of a photoionization-dominated structure the temperature profile across a uniform

nebula is expected to be fairly flat around $T_e = 20\,000\text{ K}$ (CLOUDY models at constant proton density, see below). We will also argue in Section 4, in a comparison between the spatio-kinematical data and the structure of model nebulae, that the physical conditions must be quite uniform across the cores of the nebulae, at least when averaged over 1-arcsec scales.

We used the relative intensities between H I recombination lines to evaluate errors in flux calibration. The errors stem from variations in slit positions for different frames, approximate estimations of standard star fluxes, and unresolved atmospheric transmission features. A restricted range in the J window including Pa β at 1.282 μm and the $3^3\text{S}-4^3\text{P}$ He I transition at 1.2792 was also observed in both nebulae with CGS4 in grating mode. Atmospheric transmission is quite good for Pa β , and it is a bright line observed at a very good signal-to-noise ratio. Pa β was therefore used as the flux reference H I line. On the other hand, Pa β is appreciably more affected by extinction than the longer wavelength IR lines, but its dereddened flux can be estimated from free-free radio continuum maps. We used the relation given by Milne & Aller (1975) to estimate the total H β flux from the 5-GHz free-free continuum measurement. We follow similar assumptions as in AH88, that the He abundance relative to H I is 18 per cent, and the fraction of the He atoms that are doubly ionized is 75 per cent. The total Pa β flux can then be estimated from the emissivity tables given by Hummer & Storey (1987), assuming Case B. For the hydrogen lines with He I blending we

Table 1. Ionic abundances by number for NGC 6302 and 6537, relative to solar values.

| | | $\lambda[\mu\text{m}]$ | NGC 6302 | | NGC 6537 | | IP eV | atomic data ^c |
|---------|---------------------------------------|------------------------|---|------------------------|---|------------------------|------------|-----------------------------|
| | | | I_{dered} $\text{W m}^{-2}\text{sr}^{-1}$ | abundance ^d | I_{dered} $\text{W m}^{-2}\text{sr}^{-1}$ | abundance ^d | | |
| H I | 3–5 | 1.282 | 4.15×10^{-5} | – | 4.73×10^{-5} | – | 13.6 | 1 |
| He I | $3^3\text{S}-4^3\text{P}$ | 1.253 | 5.89×10^{-7} | 0.47 | 3.23×10^{-7} | 2.68 | 24.6 | 2 |
| He II | 6–7 | 3.0917 | 1.49×10^{-5} | 1.38 | 1.62×10^{-5} | 1.60 | 54.4 | 1 |
| Ne II | $2^2\text{P}_{3/2}-2^2\text{P}_{1/2}$ | 12.81 | 1.21×10^{-4} | 0.36 | 4.24×10^{-5} | 0.17 | 21.6 | 3 |
| Ne III | $3^2\text{P}_{2-3}\text{P}_1$ | 15.5 | $7.73 \times 10^{-4a'}$ | 1.2 | – | – | 41.0 | 4 |
| Ne III | $3^1\text{P}_1-3^1\text{P}_0$ | 36.0 | $4.27 \times 10^{-5a'}$ | 0.9 | – | – | 41.0 | 4 |
| Ne V | $3^1\text{P}_1-3^1\text{P}_2$ | 14.32 | 1.42×10^{-3a} | 0.36 | 4.75×10^{-4b} | 0.13 | 97.1 | 5 |
| Ne V | $3^3\text{P}_{0-3}\text{P}_1$ | 24.31 | 5.31×10^{-4a} | 0.37 | 2.60×10^{-4b} | 0.19 | 97.1 | 5 |
| Ne VI | $2^2\text{P}_{1/2-2}\text{P}_{3/2}$ | 7.64 | 1.49×10^{-3} | 0.18 | 4.89×10^{-4} | 0.12 | 126 | 6 |
| Na VI | $3^1\text{P}_1-3^1\text{P}_2$ | 8.64 | 2.20×10^{-5} | 0.33 | 8.95×10^{-6} | 0.15 | 138 | 5 |
| Na VII | $2^2\text{P}_{1/2-2}\text{P}_{3/2}$ | 4.690 | 1.89×10^{-5} | 0.12 | – | – | 172 | 7 |
| Mg V | $3^2\text{P}_{2-3}\text{P}_1$ | 5.608 | 7.99×10^{-5a} | 0.11 | – | – | 109 | 4 |
| Mg VII | $3^1\text{P}_1-3^1\text{P}_2$ | 5.502 | 6.15×10^{-5a} | 4.9×10^{-2} | – | – | 187 | 5 |
| Mg VIII | $2^2\text{P}_{1/2-2}\text{P}_{3/2}$ | 3.028 | 8.55×10^{-6} | 2.8×10^{-3} | – | – | 225 | 6 |
| Al V | $2^2\text{P}_{3/2-2}\text{P}_{1/2}$ | 2.883 | 5.86×10^{-8} | 1.0×10^{-3} | – | – | 120 | 3 |
| Al VI | $3^2\text{P}_{2-3}\text{P}_1$ | 3.659 | 6.66×10^{-7} | 1.9×10^{-3} | – | – | 154 | 4 |
| Si VI | $2^2\text{P}_{3/2-2}\text{P}_{1/2}$ | 1.96 | 1.11×10^{-4} | 0.22 | 5.88×10^{-5} | 0.13 | 167 | 3 |
| Si VII | $3^2\text{P}_{2-3}\text{P}_1$ | 2.48 | 9.70×10^{-5} | 0.14 | 1.59×10^{-6} | 2.6×10^{-3} | 205 | 4 |
| Si IX | $3^1\text{P}_{0-3}\text{P}_1$ | 3.934 | 1.42×10^{-7} | 3.0×10^{-5} | – | – | 303 | 5 |
| S III | $3^1\text{P}_1-3^1\text{P}_2$ | 18.71 | 4.17×10^{-5b} | 0.11 | 7.68×10^{-5b} | 0.22 | 23.3 | 8 |
| S IV | $2^2\text{P}_{1/2-2}\text{P}_{3/2}$ | 10.50 | 2.08×10^{-4} | 0.13 | 2.91×10^{-4} | 0.38 | 34.8 | 9 |
| Ar III | $3^2\text{P}_{2-3}\text{P}_1$ | 9.01 | 7.66×10^{-5} | 0.38 | 3.44×10^{-5} | 0.19 | 27.6 | 8 |
| Ar V | $3^1\text{P}_1-3^1\text{P}_2$ | 7.91 | 4.29×10^{-5} | 8.4×10^{-2} | 2.91×10^{-5} | 6.2×10^{-2} | 59.8 | 8 |
| Ar V | $3^3\text{P}_{0-3}\text{P}_1$ | 13.11 | 2.09×10^{-5} | 5.1×10^{-2} | 2.22×10^{-5} | 5.8×10^{-2} | 59.8 | 8 |
| Ar VI | $2^2\text{P}_{1/2-2}\text{P}_{3/2}$ | 4.528 | 1.37×10^{-4} | 0.11 | 3.04×10^{-4} | 0.32 | 75.0 | 10 |
| K III | $2^2\text{P}_{3/2-2}\text{P}_{1/2}$ | 4.616 | 1.52×10^{-6} | 0.20 | 5.09×10^{-7} | 7.3×10^{-2} | 31.6 | 11 |
| K VII | $2^2\text{P}_{1/2-2}\text{P}_{3/2}$ | 3.189 | 1.32×10^{-6} | 3.3×10^{-2} | 9.83×10^{-7} | 2.7×10^{-2} | 99.9 | 10 |

^a ISO measurement, Pottasch et al. (1996).

^{a'} Pottasch & Beintema (1997).

^b Rowlands et al. (1994).

^c The collision strengths were for the most part taken from the IRON project. 1, Hummer & Storey (1987); 2, Smits (1991); 3, Saraph & Tully 1994; 4, Butler & Zeippen (1994); 5, Lennon & Burke (1994); 6, Zhang, Graziani & Pradhan (1994); 7, Ferland (1996, as used in CLOUDY); 8, Galavís et al. (1995); 9, Johnson et al. (1986); 10, Saraph & Storey (1996); 11, Pelan & Berrington (1995).

^d Ionic abundance relative to the total solar abundance of each element, or (Nx/Np)/solar. Solar abundances from Grevesse & Anders (1989), Grevesse & Noels (1993).

used the He I emissivities of Smits (1991), normalized to He I $3^3\text{S}-4^3\text{P}$.

Gomez et al. (1989) present a Very Large Array (VLA) map of NGC 6302 at 5 GHz, which allows extinction estimates for a 3×3 arcsec² beam. Our measured flux for Pa β of 3.9×10^{-15} W m⁻² gives $A_V = 3.7$ in the central region, with $S(5 \text{ GHz}) = 375$ mJy (over the same region we have 1.6×10^{-16} W m⁻² for the He I $3^3\text{S}-4^3\text{P}$ observed flux). Although this value is not in agreement with the mean value for the whole nebula of $A_V = 2.65$ (Pottasch et al. 1996), it agrees with the conclusion by AH88 that extinction in the central regions of NGC 6302 is higher than the mean by 1.3 mag. Unfortunately no VLA maps are available for NGC 6537, but the estimations of AH88 give $A_V = 4$, very close to the value for NGC 6302 (for which they estimate $A_V = 4.3$). We fixed the extinction in NGC 6537 to $A_V = 3.5$ magnitudes by requiring the unblended Br α to Pa β flux ratio to match the ratio of their emissivities at 20 000 K (from Hummer & Storey 1987).

Unresolved atmospheric transmission (AT) troughs can be recognized from an atmospheric transmission model for Mauna Kea (based on the HITRAN data base, Rothman et al. 1992). We took Pf5–10 as typical, because it lies in a trough, but its predicted flux was very close to the observed one. Unresolved atmospheric transmission features are, however, a source of uncertainty in the low-resolution flux measurements, as shown by AH88 in the case of [Si VI], which can be completely absorbed by atmospheric H₂O. We used the extinction law given by Rieke & Lebofsky (1985), and the dereddened and deblended H I fluxes are at most 20 per cent different from the values expected from the radio map in the case of NGC 6302. Observing from Mauna Kea, with a low column of precipitable water vapour, minimizes the effect of AT troughs.

The emission measure integrated along the line of sight, $EM = \int ds N_p N_e$, can be estimated from the intensity of hydrogen emission lines (e.g. Osterbrock 1989),

$$I = \int ds N_p N_e (h\nu\alpha_{\text{eff}})/(4\pi), \quad (1)$$

where α_{eff} is the effective recombination coefficient for Pa β (Hummer & Storey 1987). The Pa β line flux from the central 3×3 arcsec² in NGC 6302 is $F_{\text{Pa}\beta} = 3.9 \times 10^{-15}$ W m⁻², giving $EM = 5.6 \times 10^{35}$ m⁻⁵. For NGC 6537, $F_{\text{Pa}\beta} = 3.8 \times 10^{-15}$ W m⁻², and $EM = 5 \times 10^{35}$ m⁻⁵.

3.2 Abundance patterns and photoionization models

Table 1 lists the deblended and dereddened surface brightnesses through the central CGS4 row (3×3 arcsec² square aperture), together with the abundances calculated using the atomic data referenced there. The [Si VI] and [Si VII] fluxes were derived from UKIRT observations in April 1986 with the CVF on UKT9, using a 19.6-arcsec circular aperture. We also used some fluxes from Pottasch et al. (1996) and Rowlands et al. (1994), as indicated in Table 1. We estimated the average intensity in the central 3×3 arcsec² by using the spatial information from our grating and echelle CGS4 spectra (see the end of Appendix A). The fluxes obtained with large beams were scaled by a factor 0.4 for NGC 6302 and 0.58 for NGC 6537, to estimate the corresponding fluxes in the central 3×3 arcsec² (except for [S III], for which we used a factor of 0.15 for NGC 6302, and 0.37 for NGC 6537).

Although we list only ionic abundances, we can draw some conclusions about abundance patterns from those elements having several observed ionization stages and reliable line fluxes.

Magnesium seems to be slightly depleted relative to solar, but not as strongly as aluminium. Potassium shows a very small ionization fraction in K VII, when compared with Ne V at a similar ionization potential, or to Na VI and Na VII. Although a somewhat higher abundance in neon is expected in Type I PNe (Corradi & Schwarz 1993), it could be that potassium is slightly depleted, because no special overabundance is expected in sodium.

We also used CLOUDY 90.03 (Ferland 1996) to construct a photoionization model of NGC 6302. The nebula is simulated as a spherically symmetric shell, although the fluxes of emission lines are calculated by truncating the shell in order to simulate the long-slit observations. The radiation field of the central star is assumed to be that of a blackbody. No systematic depletion of metals on grains was assumed, principally because little is known about dust survival in PNe. None the less, the abundances of elements likely to be depleted were allowed to vary, in particular magnesium shows an important line that should be reproduced accurately. The abundances were otherwise taken as solar. We also varied the filling factor, the temperature of the blackbody and the inner radius of the nebula. The optimization driver of CLOUDY was constrained by the fluxes of IR coronal ions and the H II column density (estimated from the observed emission measure, with $N_e = 1.8 \times 10^4$ cm⁻³).

The main problem in using CLOUDY for this application is that we are probing the central region of NGC 6302, whereas CLOUDY calculates the fluxes from the whole nebula. The cumulative fluxes versus radius could be matched with our spectra, leaving the cut-off radius as yet another free parameter. But one way around this problem is to reproduce the fluxes relative to another

Table 2. CLOUDY output from the best-fitting models for NGC 6302 and 6537. Columns 2–5 list ionic line fluxes relative to [Ar VI] $4.53 \mu\text{m} = 1.00$.

| | NGC 6302 | | NGC 6537 | |
|-----------------|-------------------------|--|-------------------------|--|
| Filling factor | 0.70 | | 0.58 | |
| Inner radius | 6.2×10^{15} cm | | 3.8×10^{15} cm | |
| Blackbody T_* | 241 000 K | | 156 000 K | |
| Luminosity | 8500 L _⊙ | | 8500 L _⊙ | |
| Mg abundance | ≈0.5 solar | | – | |
| Al abundance | ≈0.01 solar | | – | |

| ID λ (μm) | NGC 6302 | | NGC 6537 | |
|--------------------------------|-----------------------|-----------------------|-----------------------|-----------------------|
| | Model | Obs. | Model | Obs. |
| [Ne v] 14.3 | 5.7 | 10 | 3.6 | 1.6 |
| [Ne v] 24.2 | 1.8 | 3.9 | 1.2 | 0.86 |
| [Ne vi] 7.64 | 8.6 | 11 | 1.3 | 1.6 |
| [Na vii] 4.69 | 7.6×10^{-2} | 0.14 | – | – |
| [Mg v] 5.60 | 0.30 | 0.60 | – | – |
| [Mg vii] 5.51 | 0.31 | 0.40 | – | – |
| [Mg viii] 3.03 | 5.0×10^{-2} | 6.0×10^{-2} | – | – |
| [Al v] 2.9 | 6.0×10^{-4} | 5.0×10^{-4} | – | – |
| [Al vi] 3.66 | 4.8×10^{-3} | 5.0×10^{-3} | – | – |
| [Si vi] 1.96 | 0.80 | 0.80 | 9.0×10^{-2} | 0.19 |
| [Si vii] 2.47 | 0.32 | 0.71 | 2.5×10^{-3} | 5.2×10^{-3} |
| [Si ix] 3.93 | 1.2×10^{-3} | 1.0×10^{-3} | – | – |
| [S iv] 10.5 | 2.26 | 1.52 | 2.89 | 0.96 |
| [Ar v] 7.91 | 9.3×10^{-2} | 0.30 | 0.12 | 9.6×10^{-2} |
| [Ar v] 13.1 | 7.6×10^{-2} | 0.15 | 9.5×10^{-2} | 7.3×10^{-2} |
| [Ar vi] 4.53 | 1.00 | 1.00 | 1.00 | 1.00 |
| [Na vi] 8.64 | 8.3×10^{-2} | 0.16 | 1.7×10^{-2} | 2.9×10^{-2} |
| [K vii] 3.19 | 5.2×10^{-2} | 1.0×10^{-2} | 2.5×10^{-2} | 3.2×10^{-3} |
| N(H II) ^a | 1.49×10^{21} | 1.55×10^{21} | 1.33×10^{21} | 1.40×10^{21} |

^a Column density of H⁺ in cm⁻² integrated outwards from the central star.

ionic line. We took [Ar VI] at $4.53 \mu\text{m}$ as the reference line, and the CLOUDY output can be seen in Table 2, as well as the best-fitting values for the free parameters. A total hydrogen volume density of $\log(N_{\text{H}}) = 4.2$ was given as input, together with a relative helium abundance by number of 0.14 (using 0.18, as reported by Aller et al. 1981 and as derived in this work, does not change the results). The total luminosity of the central star was fixed to be $8500 L_{\odot}$, simply because it is close to a standard PN value, although Pottasch et al. (1996) estimate $L = 11\,000 L_{\odot}$ for a distance of 1.6 kpc (Gomez et al. 1993). Using $11\,000 L_{\odot}$ leaves the model unchanged. The calculation stopped at an outer radius of 1.2×10^{17} cm because the lower-limit electron temperature of the package of 4×10^3 K was reached.

The best-fitting blackbody temperature is about 250 000 K. This is to be compared with the very high values of 450 000 K found by Lamé & Ferland (1991), and 380 000 K by Pottasch et al. (1996). One important new datum used here is the [Si IX] flux, which is actually quite low and would be significantly overestimated by models with T_{\star} higher than 250 000 K. This result has already been mentioned by Marconi et al. (1996) in their study of the Seyfert 2 galaxy NGC 1068. Arguing against the production of Si IX by hot stars, they take as an example the nucleus of NGC 6302, and model the absence of [Si IX] from their NGC 6302 spectra by putting an upper limit on T_{\star} of 250 000 K (using CLOUDY as well). The central star in NGC 6302 is thus probably not as hot as previously thought, $T_{\star} = 380\,000$ K overestimates the [Si IX] flux by a factor of 60 (with an optimized filling factor of 0.16, and an inner radius of 3.1×10^{16} cm). But could silicon be depleted? The CLOUDY model shows that 70 per cent of all silicon nuclei are distributed in Si V, Si VI and Si VII. The match to the [Si VI] and [Si VII] lines should provide a good grip on the silicon abundance, and they are approximately reproduced using a solar silicon abundance.

Together with the model results for NGC 6302, Table 2 shows the result of a CLOUDY model that reproduces the lines observed from NGC 6537, with a central star temperature of 156 000 K (using similar inputs as for NGC 6302, with $\log(N_{\text{H}}) = 4.2$; the calculation stopped because the lower limit electron temperature of the package was reached). [Al VI] was not detected towards NGC 6537, but its predicted flux assuming a solar Al abundance would be 5.7×10^{-2} times the [Ar VI] flux (which is $6.4 \times 10^{-14} \text{ W m}^{-2}$ for the central $3 \times 3 \text{ arcsec}^2$ in NGC 6537). As the [Al VI] frame shows Hu 17 close to the detection limit, with a flux 5.4×10^{-4} times the [Ar VI] flux, we can conclude that Al is depleted to less than one hundredth solar.

The abundance ratios of consecutive stages of ionization as a function of ionization potential are, in the case of photoionization, a probe of the high-energy flux from the central star. Fig. 5(a) shows the ionization distribution calculated from the observed fluxes. We can use the CLOUDY model for NGC 6302 to construct a similar curve, shown in Fig. 5(b). The curve is in remarkable agreement with the observations, except for the silicon ions. The Mg VIII to Mg VII ratio also argues for a T_{\star} of about 250 000 K. Such good agreement is surprising considering all the approximations involved in the modelling. In a complete model of the nebula, a number of arbitrary assumptions about the recombination data have to be made from the very first ionization stage. The abundance ratio of consecutive stages of ionization is inversely proportional to the total recombination coefficient, and little information is available on the dielectronic part, especially at nebular temperatures. But even if the atomic parameters were known with sufficient accuracy, as well as the temperature of the coronal line region, the spectrum of the central star may differ significantly from a blackbody.

With the cautions noted above (that a match between model and observed fluxes is acceptable within a factor of ~ 2), the abundances computed by CLOUDY confirm the patterns from the direct estimate. For both NGC 6302 and 6537, aluminium is depleted to one hundredth of the solar value, or even less. The magnesium abundance is about half solar in NGC 6302. Neon seems to be overabundant in NGC 6302, but by less than a factor of 2 relative to the solar value. It could be that potassium is depleted to one fifth of the solar abundance in NGC 6302 as well as in NGC 6537, although only one line is available. The uncertainties in the photoionization model may be reflected in the discrepant Si VII to Si VI abundance ratio (which is sensitive to extinction) and the model deficiency in [Ar V] and in the sodium lines, but in all cases the discrepancies are less than a factor of 2–3.

Aller et al. (1981) found that Ca was depleted to one tenth solar in NGC 6302, while Oliva et al. (1996) estimated Ca to be depleted by a factor ~ 20 , and Fe by a factor of $\sim 10^3$ (see also Shields 1983 for depletion patterns in other PNe). It could be that titanium is also strongly depleted. According to the CLOUDY model, the flux of [Ti VI] $1.7 \mu\text{m}$ should be a little less than that of Bry, at about one fiftieth of [Ar VI], but no spectrum in the H window has been published for NGC 6302. However, most of the titanium should be in Ti VII or Ti VIII, and the ground state, magnetic dipole, [Ti VII] $4144.2\text{-}\text{\AA}$ line is missing in the spectrum published by Aller et al. (1981). So it seems likely that Ti is strongly depleted. The strong depletion of Al, and possibly of Ti,

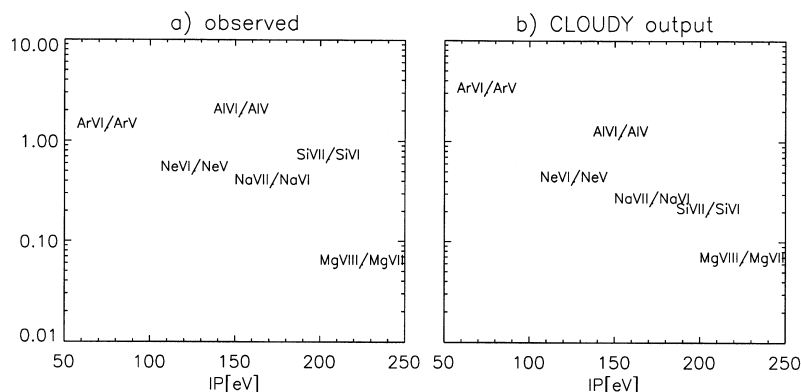


Figure 5. Ionization distribution for NGC 6302. The abscissa is the photon energy required to ionize the lower stage of ionization, and the ordinate is $N(X^{+i+1})/N(X^{+i})$. The uncertainty in the observed ratios can be up to a factor of 2.

implies that some dust is well mixed with the gas phase, in the form of Ti and Al compounds, such as perovskite, CaTiO_3 , and corundum, Al_2O_3 , which have very high sublimation temperatures. Gail & Sedlmayr (1998) argue that the first condensates in circumstellar outflows are Ti compounds, which could be nucleation sites for the aluminium compounds and silicates. When the AGB ejecta are heated to nebular temperatures and exposed to hard UV radiation, grain ablation could explain the observed depletions. Kingdon & Ferland (1997 and references therein) suggest that strong ionic depletions are indicative of dust survival in the ionized phase of PNe. Examples are Fe depletions inferred from Fe VII, which requires radiation harder than 100 eV. We note here that since 154 eV is required to ionize Al V, the Al depletion derived for NGC 6302 from Al VI provides evidence for dust survival in very hard radiation field environments. Pwa et al. (1984, 1986) also measured Al depletions of a factor ~ 100 for NGC 6543 and a factor ~ 10 for BD + 30°3639, from *IUE* observations of Al II and Al III absorption lines.

It would seem that photoionization models can account for the observed ionization distribution in broad terms. Zhekov & Perinotto (1996) attempted to model the IR coronal line emission from high excitation PNe for the case of a collisionally excited plasma. They used an interacting wind model, following Weaver et al. (1977), in which the slow AGB wind is accelerated into a shock by the fast white dwarf wind. The hot bubble grows as the shock expands and ‘vaporizes’ material from the cold shell. After working out the temperature structure of the bubble, they calculated its coronal line emission using the hot plasma emissivities. But their predicted fluxes are in strong disagreement with those observed from NGC 6302, e.g. the predicted [Si IX] and [Mg VIII] fluxes should be of the same order according to their model.

3.3 The progenitor of NGC 6302

In this section we present arguments for the progenitor of NGC 6302 having a lower zero-age main-sequence (ZAMS) mass than previously thought. The total luminosity of the central star can be estimated from a sum of all flux measurements of NGC 6302 from the UV to the infrared (Pottasch et al. 1996 and references therein.). For a distance of 1.6 kpc (as determined by Gomez et al. 1993 using VLA observations of the expansion rate), the luminosity of the central star is about $1.1 \times 10^4 L_\odot$. We can now locate the star in the Hertzsprung–Russell (H–R) diagram and compare with the theoretical tracks of Blöcker (1995). A temperature of 380 000 K would locate the star on the track of a hydrogen-burning model with a $7 M_\odot$ initial mass (and a core mass of $M_H = 0.940 M_\odot$) 60 yr or so after leaving the AGB. But our estimate of 250 000 K would fall on a track between the Blöcker (1995) models with $(M_{\text{ZAMS}}, M_H) = (4 M_\odot, 0.696 M_\odot)$ and $(5 M_\odot, 0.836 M_\odot)$, or a 4–5 M_\odot initial mass, for either the hydrogen-burning models or the born-again helium burners. It is difficult to distinguish between the two burning modes, as the time-scale is slower in the helium burners by a factor of 3 only. If the bulk of the nebular material was ejected at the time the star left the AGB, the age of about 2000 yr necessary to account for the size of the NGC 6302 of 10^{17} cm at an expansion speed of 10 km s^{-1} may be better explained in terms of the born-again models of Blöcker (1995). The PN progenitor could have had a ZAMS mass of $\sim 4 M_\odot$ and have left the AGB on the verge of a thermal pulse, since the time-scale for a straight evolution from the AGB as a hydrogen burner is only 700 yr (alternatively the star

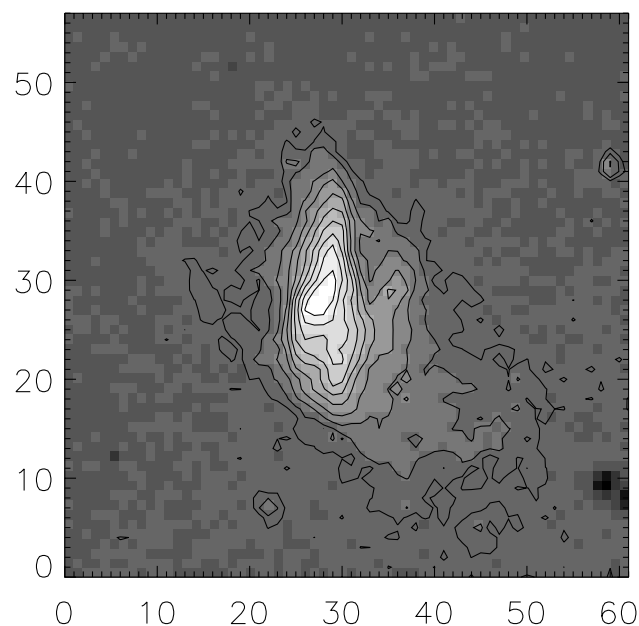


Figure 6. IRCAM image of the 3.3- μm UIR-band emission in NGC 6302. Pixel numbers are plotted along the axes. The pixel size was 0.6 arcsec and the width of the narrow-band filter was 0.3 μm . The contour levels are 0.05, 0.1, 0.2, 0.3, 0.4, 0.5, 0.6, 0.7, 0.8, 0.9 of the peak flux, to allow comparison with the VLA 6-cm map from Gomez et al. (1989). North is down and east is to the right.

could have left the AGB just after a thermal pulse, and evolved on a similar time-scale as the born-again case, although Blöcker does not provide tracks for this case).

The OH maser observed in NGC 6302 by Payne, Phillips & Terzian (1988) provides evidence for an oxygen rich environment, as does the *ISO* detection of mid-IR crystalline silicate emission bands (Waters et al. 1996), and yet the nebula shows the family of ‘unidentified infrared’ (UIR) emission bands (Roche & Aitken 1986), attributed to carbon-based molecules (Duley & Williams 1981; Léger & Puget 1984). The OH maser emission seems to come from the material surrounding the core of the nebula, because the cuts in velocity published by Payne et al. (1988) peak at different positions around the centre, over about 8 arcsec. On the other hand, the 3.3 μm UIR emission band is centrally peaked, as can be seen on our IRCAM frame shown in Fig. 6. The extent of the UIR emission can be compared with the VLA map of Gomez et al. (1989). The UIR bands are typical of C-rich PNe (Cohen et al. 1986), and these observations support a scenario in which the progenitor of NGC 6302 was an M giant that went through a carbon transition at the very end of its evolution, as is analysed in detail by Frost et al. (1998). However, maser amplification requires particular conditions, and therefore does not systematically trace the distribution of O-rich material, and the evidence for a stratification in C/O chemical balance is only marginal until high-resolution OH observations are available and a model is constructed. None the less NGC 6302 clearly includes both C- and O-rich environments. Values of $\text{C}/\text{H} = 4.4 \times 10^{-4}$, $\text{N}/\text{H} = 9.2 \times 10^{-4}$ and $\text{O}/\text{H} = 5.0 \times 10^{-4}$ have been derived for NGC 6302 by M. J. Barlow, using the UV and optical relative line intensities measured by Barral et al. (1982) and Aller et al. (1981), respectively. Collisionally excited lines were used to derive the abundances of the singly, doubly and triply ionized species, while the 6h–5g recombination lines in the 4600-Å region were used to

derive the abundances of the four-times ionized species, as in Clegg et al. (1987).

Synthetic AGB evolution models (Renzini & Voli 1981) are compilations of model results from full evolutionary calculations, and allow searches over a continuous range of progenitor masses. Using an adaptation of the synthetic AGB model by Groenewegen & de Jong (1993), we can search for a progenitor mass that accounts for the properties of NGC 6302. In this model we do not constrain envelope burning to stop at the same time as dredge-up (e.g. Frost et al. 1998). Many uncertainties affect the treatment of hot bottom burning (HBB), in this case one of them being the arbitrary onset of HBB for core masses greater than $0.8 M_{\odot}$ ¹. But our purpose here is to illustrate an alternative argument to the post-AGB tracks for NGC 6302 having a relatively low progenitor mass. The above uncertainties in the treatment of HBB would decrease the lower mass limit of the range of initial masses that account for the composition of NGC 6302. Fig. 7 shows the time after the C transition as a function of initial mass for stars at the end of the AGB, as well as the averaged C/O and N/O ratios over the last 10 000 yr of mass loss. Towards $6 M_{\odot}$ the time after the C-transition is too long, the carbon-rich nebular material having been ejected at most over 2000 yr. Below $4.2 M_{\odot}$ HBB is not activated and the envelope composition is dominated by the dredge-up of carbon. Thus, in terms of the quenching of HBB at the end of the AGB evolution of the progenitor, the main-sequence mass of the progenitor of NGC 6302 would lie between $4 M_{\odot}$ and $5 M_{\odot}$ to account for the transition in C/O ratio. This mass range is also confirmed by the observed gas phase abundances, and is in independent agreement with the comparison of the temperature of the central star and the post-AGB tracks of Blöcker (1995). Fig. 8 shows the synthetic evolution of a $4.45 M_{\odot}$ model that matches the observational requirements. It can be seen that the star goes through a C transition over the last 2000 yr. The final C/O ratio is as high as that found in circumstellar environments that show the UIR bands (and not SiC, e.g. Barlow 1983, Roche 1989).

4 KINEMATICAL STRUCTURE OF THE CORES OF NGC 6302 AND 6537

4.1 Velocity profiles from the echelle spectra and the observed ionization-stage stratification

The velocity profiles along the echelle slit are shown in Fig. 9 for NGC 6302. A radically different velocity structure can be seen when comparing the coronal ions with Br γ for the \perp slit orientation, along the bipolar axis. The ions show an outflow type of profile, whereas Br γ displays the characteristic X-shaped profile obtained for optical recombination lines, and for [N II] by Elliot & Meaburn (1977). This difference can be checked at offset -8 arcsec, where the double Gaussian fit to the Br γ line profile has clearly separated centroids, whereas [Mg VIII] or [Ar VI] are centrally peaked (the maxima at each offset are shown by crosses). The \parallel slit orientation shows narrow and centrally peaked velocity

¹The lack of a continuous transition would preclude the existence of type IIa PNe, with $\log(N/O) > -0.6$ (as defined by Faúndez-Abans & Maciel 1987), which in Groenewegen & de Jong (1993) are mainly obtained at high initial metallicity, but are none the less observed to exist in the LMC (Leisy & Dennefeld 1996). A limiting core mass of $0.8 M_{\odot}$ for HBB also constrains N enrichment to occur for stars close to the 2nd dredge-up critical mass (Becker & Iben 1979), which does not reproduce the population of C-rich Type I PNe, except for progenitor masses greater than $6 M_{\odot}$.

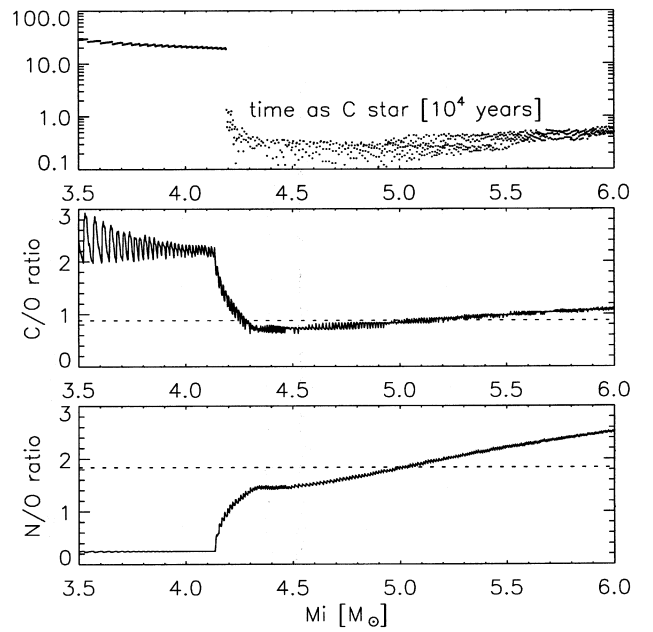


Figure 7. The upper plot shows the variation of the time spent in the C star phase at the end of the AGB as a function of initial mass. The lower two plots show the C/O and N/O ratios in the ejecta averaged over the last 10 000 yr of evolution, and the horizontal dashed lines correspond to gas-phase measurements of the corresponding ratios (see text).

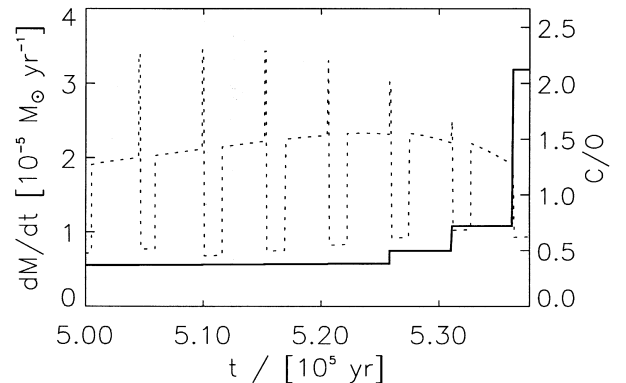


Figure 8. Schematic evolution of a $4.45 M_{\odot}$ star at the end of the AGB. The dotted line is the mass-loss rate (left-hand scale) and the solid line is the surface C/O ratio (right-hand scale). The last thermal pulse changes the C/O chemical balance of the envelope of the star, approximately 2000 yr before envelope ejection.

profiles, in particular for [Mg VIII]. Br γ is less extended in the \parallel direction, consistent with the structure expected from a bipolar flow in the \perp direction.

For NGC 6537, velocity profiles with the \parallel slit orientation only are available. Fig. 10 shows that they have a similar structure to the \parallel slit orientation in NGC 6302. The lines are also quite narrow.

Table 3 lists the widths of the lines (FWHM, the instrumental line widths were subtracted in quadrature) obtained by fitting the spectra extracted from the collapsed slits. The uncertainties stem from the instrumental linewidths. The linewidths from the arc lamp spectra for the two [Mg VIII] and the [Ar VI] echelle frames are consistent with $\Delta V = 26 \pm 1 \text{ km s}^{-1}$ over the central third of the array, although the [Ar VI] arc frame had a 20 km s^{-1} wide line

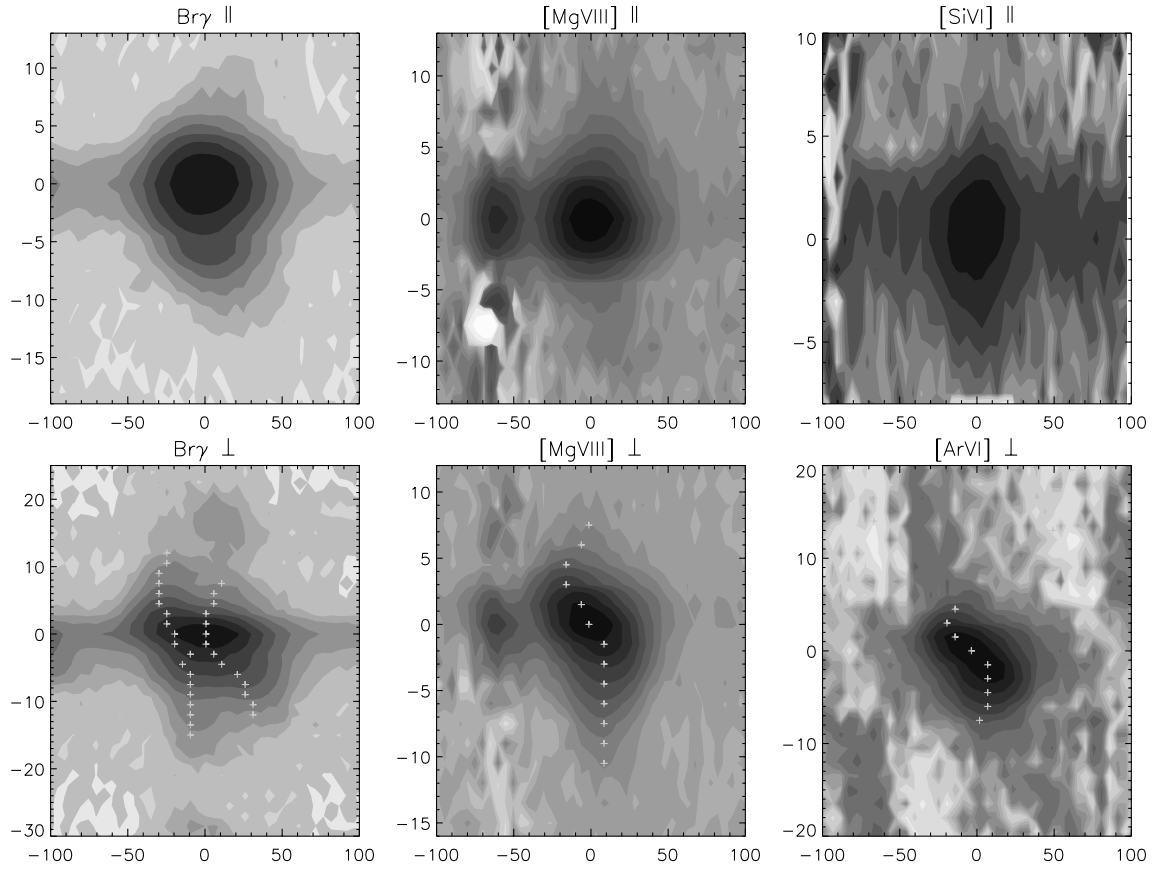


Figure 9. Results of our echelle observations of NGC 6302. The two slit positions are referred to as \parallel for the direction along the waist of the nebula, and \perp along the bipolar axis. From left to right are shown Br γ , [Mg VIII] 3.028 μm and [Si VI] 1.963 μm or [Ar VI] 4.528 μm . The y-axis is the offset along the slit in arcsec, and the x-axis shows the velocity in the rest frame of the object (km s^{-1}). The contour levels are at the maximum flux density times powers of $1/2$. The crosses correspond to the maxima for each row. East is towards positive offsets in the frames with the \perp slit orientation.

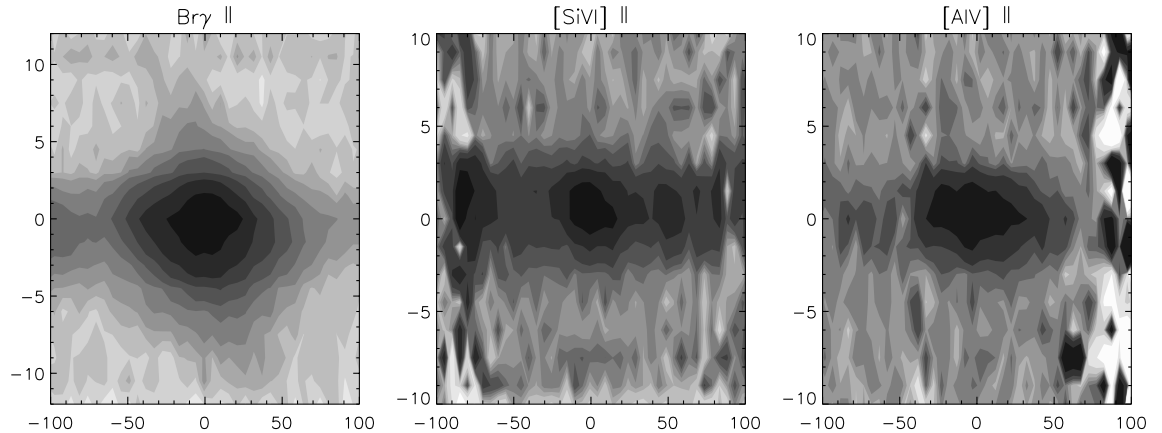


Figure 10. Results of our echelle observations of NGC 6537. From left to right are shown Br γ , [Si VI] 1.963 μm and [Al IV] 2.883 μm . The slit was oriented along the waist of the nebula. The y-axis is the offset along the slit in arcsec, and the x-axis shows the velocity in the rest frame of the object (km s^{-1}). The contour levels are at powers of $(1/2)$ times the maximum flux density for each frame.

in the centre. But it is clear that the lines are very narrow indeed, and might even not be resolved in the case of [Si VI] in NGC 6537.

The velocity profiles give evidence for stratification in NGC 6302, as can be seen in Fig. 11. The contour at half maximum corresponding to [Mg VIII] (dotted line), at $IP = 224.95$ eV, is less extended than those of [Ar VI], $IP = 75.04$ eV, and [Si VI],

$IP = 166.77$ eV. The nebular emission in each frame did not necessarily peak on the same row, which affects the registration of the contours between different observations. The relative positioning of the contours is also affected by the limited spatial resolution of about 1.5 arcsec along the slit, and by the velocity resolution of ~ 10 km s^{-1} per pixel along the dispersion axis. It can be noted

Table 3. FWHM linewidths ΔV in km s^{-1} , together with the ionization potential (IP , eV) required to produce the observed ion, and the wavelength λ in μm .

| | Bry | [Mg VIII] | [Si VI] | [Ar VI] | [Al V] |
|-----------------------------|-------|-----------|---------|---------|--------|
| λ [μm] | 2.166 | 3.028 | 1.963 | 4.528 | 2.883 |
| IP [eV] | 13.6 | 225 | 167 | 75.0 | 154 |
| NGC 6302 | | | | | |
| ΔV_{\parallel} | 31(5) | 18(2) | 22(5) | – | – |
| ΔV_{\perp} | 41(5) | 24(2) | – | 27(5) | – |
| NGC 6537 | | | | | |
| ΔV_{\parallel} | 39(5) | – | 14(10) | – | 30(20) |

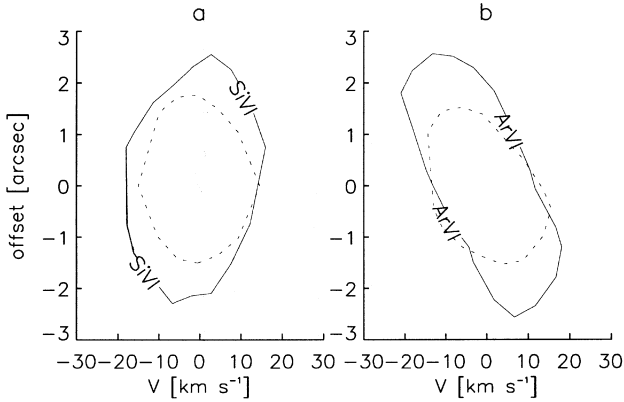


Figure 11. Spatial and velocity extent of [Mg VIII] (dotted line), [Si VI] and [Ar VI]. The contours are taken at half maximum (a) for the slit oriented along the dusty lane, (b) for the slit oriented along the bipolar axis. The registration of the contours is uncertain to 0.1–0.2 arcsec.

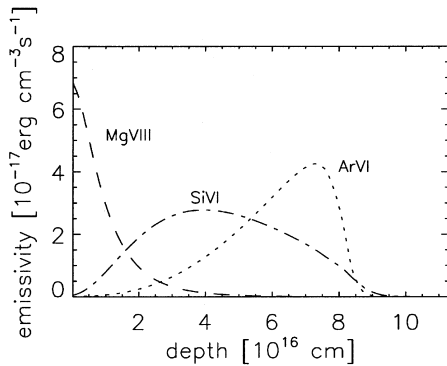


Figure 12. The ionization structure of a uniformly dense nebula as computed by CLOUDY, with the parameters of NGC 6302.

that the lower ionization species are more spatially extended than [Mg VIII], which matches the structure of a photoionized nebula, shown in Fig. 12. The velocity width of the lines also show stratification, implying that material is accelerated outwards from the nucleus.

4.2 The absence of a wind-blown cavity

Most kinematical studies of bipolar nebulae have been based on optical echelle spectroscopy of [N II] 6584 Å, which does not probe the high-excitation regions and suffers from extinction. The general structure that emerges from the optical studies is typically

a bipolar cavity surrounded by an expanding H II region, which in turn is confined by some higher density medium (sometimes detected in H I or CO). The observational results are usually compared with the interacting stellar winds model (ISW, Kwok et al. 1978), with fairly good agreement. For instance, Corradi & Schwarz (1993) studied NGC 6537 and Hb5 in [N II] and compared their results with the ISW model of Icke, Preston & Balick (1989); NGC 6537 has also been studied in [N II] by Cuesta, Phillips & Mampaso (1995) and its kinematical structure was consistent with refraction of a fast wind on the walls confining an evacuated cavity (model for Herbig–Haro objects from Cantó 1980); Bryce et al. (1996) established the velocity structure of NGC 650-1 using [N II] and [O III], and the results were in reasonable agreement with the GISW models presented in Frank & Mellema (1994). A common feature in the models quoted previously is that a hot evacuated cavity ($N_e \sim 10 \text{ cm}^{-3}$) occupies a good portion of the volume of the PN, the walls of which are expanding with velocities of order 50 km s^{-1} .

In the case of NGC 6302, the above picture would seem to be confirmed by the CGS4 + echelle observations of Bry. Fig. 9 shows that the Bry profiles double-peak further out than 8 arcsec from the nucleus, which is an indication for a possible decrease in proton density along the bipolar axis. This could also be extrapolated from the optical echelle measurements of recombination lines (Elliott & Meaburn 1977), and from the H β image of Ashley (1990), under the assumption of axial symmetry.

But the use of coronal ions as tracers of the velocity field produces quite a different picture. The observed ionization stage stratification is consistent with a CLOUDY model for a nebula at constant density (Fig. 12). We also have no indications for a torus type of structure rather than a disc around the waist of the nebula, at least at about 1-arcsec resolution, as can be seen from the frames along the dusty lane. The same situation seems to apply to NGC 6537 (Fig. 10). Additionally, the single-peaked profiles of the coronal lines out to 8 arcsec offsets along the bipolar axis (in NGC 6302, Fig. 9) show that the corresponding physical conditions cannot be that of a rarefied plasma. The detection of coronal-line emission requires $N_p \gtrsim 10^3 \text{ cm}^{-3}$ out to 10 arcsec offsets, and even higher if the decrease in ionic abundance is taken into account.²

Arguments against the existence of a sizeable evacuated cavity may also be extrapolated from the VLA 6-cm map of the central 20 arcsec of NGC 6302 by Gomez et al. (1993). The 6-cm continuum traces the emission measure across the central regions of the nebula (provided T_e is fairly uniform). Under the assumption of axial symmetry, the possibility of an extreme decrease in proton density from nebular conditions to $\sim 10 \text{ cm}^{-3}$ along the bipolar axis can be discarded (note that for a given 6-cm flux density, an increase in T_e requires an increased EM). The CGS4 + echelle results reported here confirm the filled-in picture evident from the VLA map, this time using tracers of highly excited gas. Also, early observations of PNe by Wilson (1950) showed that the central ‘cavities’ in the long slit spectra of low-ionization species (such as [O II] and [N II]) are filled-in, spatially

²Using detailed balance it is possible to determine the range in temperature and density where the predicted ratio of the flux at nebular conditions ($N_e = 18000 \text{ cm}^{-3}$ and $T_e = 20000 \text{ K}$, Section 3) to the flux at (N_e, T) would put it below the noise level. A drop in [Mg VIII] flux by a factor of 1000 corresponds to a drop in density from nebular conditions (Section 3) to $N_p \gtrsim 8 \times 10^2 \text{ cm}^{-3}$. The limiting case $N_p = 8 \times 10^2 \text{ cm}^{-3}$ corresponds to $T_e = 10^4 \text{ K}$.

and spectrally (at $\sim 10 \text{ km s}^{-1}$ resolution), by higher-ionization species such as [Ne v]. Wilson (1950) thus reported a stratification in ionization potential, including the intermediate ionization species [O III] and [Ne III].

NGC 6302 has previously been studied in [Ne v] by Meaburn & Walsh (1980). They concentrated on the detection of a fast wind in the broad wings of [Ne v], which are absent in their [N II] profiles. This discovery has been interpreted by Barral et al. (1982) in terms of the Cantó (1980) model for H–H objects. In this model, flows are generated as the stellar wind refracts on a dense disc surrounding the star and is accelerated along the walls of the bipolar nebula. The shape of the walls is determined by equating the ram pressure of the wind to that of the surrounding medium. The conclusion of Barral et al. (1982) within this model is that the dominant excitation mechanism is still radiative ionization. In this case, an altogether different model for photoionization should be considered, in which the nebula has in fact a shell structure, the hot bubble consisting only of the stellar wind itself. But the spectra of [Ne v] published by Meaburn & Walsh do not show a double-peaked structure, at a resolution of about 10 km s^{-1} . Although Meaburn & Walsh (1980) interpreted the geometry of NGC 6302 as an evacuated cavity, with [Ne v] emission originating from the walls, their results do not show the corresponding velocity profile. We believe a filled-in structure is not inconsistent with observing different velocity components, provided the nebula has a clumpy structure.

This section points towards the absence of a wind-blown cavity filled with a hot rarefied plasma, in the case of the highest excitation PN known. We suggest that the clumpiness of the nebula precludes the formation of a wind-blown cavity. This point should be further investigated to see under which conditions, if any, bipolar PNe would show signs of a hot bubble. Similar conclusions have been reached by O’Dell (1998) and Henry, Kwitter & Dufour (1999) in the case of the Helix nebula (NGC 7293), namely that the ionized phase of the nebula is a disc rather than a ring, filled by highly ionized gas. The current ISW dynamical models that account for the shaping of PNe have also been used to explain a variety of astrophysical objects, and even the collimation of jets in AGN (Icke et al. 1992) and young stellar objects (Mellema & Frank 1997). But the ISW model was built from and checked against optical studies of relatively low ionization species in PNe, and we have shown here that the observational information should be extended by studies of the cores of other nebulae in higher-excitation species.

4.3 What are the physical conditions in the fast wind?

The signal-to-noise ratio of our echelle observations of NGC 6302 in [Ar VI] and [Mg VIII] is higher than that of [Ne v] 3426 Å presented by Meaburn & Walsh. Also, Ne v has an ionization energy between that of Ar VI and Mg VIII, while the IR coronal lines and the optical [Ne v] line have similar critical densities (at 10^4 K , the IRON project collision strengths give $N_{\text{crit}}([\text{Ar VI}]) \sim 10^6 \text{ cm}^{-3}$, $N_{\text{crit}}([\text{Ne v}]) \sim 5 \times 10^6 \text{ cm}^{-3}$, $N_{\text{crit}}([\text{Mg VIII}]) \sim 10^7 \text{ cm}^{-3}$). So why are no extended wings observed in the IR coronal lines?

Without mass loading, the fast stellar wind should vary in density with angular distance in arcsec, α , from the central star approximately as $10/\alpha^2 \text{ cm}^{-3} \text{ arcsec}^{-2}$ (for $dM/dt = 10^{-8} M_{\odot} \text{ yr}^{-1}$ and $V_{\text{fw}} = 1000 \text{ km s}^{-1}$). This would not be detected in IR emission because of insufficient collisional excitation, leading to a very-low-excited-ion column density. But the physical conditions

where the broad wings originate could be intermediate between the fast stellar wind and nebular conditions. Let us consider the implications of assuming collisional excitation for the fast wind observed by Meaburn & Walsh (1980). For the $^3\text{P}_2-^1\text{D}_2$ [Ne v] 3426-Å transition, the line intensity can be written as

$$I_{i-j} = \frac{1}{4\pi} \int \epsilon ds b A_{ij} h \nu n_{\text{up}} N_{\text{o}}, \quad (2)$$

where b is the branching ratio, ϵ the filling factor, n_{up} is the fraction of ions in the upper level, and N_{o} is the number density of ions. We have given a number of justifications for the fast wind coexisting with the denser clumps, which occupy a significant fraction of the volume ($\epsilon \sim 0.5$), so the filling factor of the fast wind should be similar. The ratio of the intensity from the narrow component of the line to that from the fast wind will be given approximately by

$$\frac{I_{\text{narrow}}}{I_{\text{wings}}} \approx \frac{(n_{\text{up}} N_{\text{p}})_{\text{narrow}}}{(n_{\text{up}} N_{\text{p}})_{\text{wings}}} \quad (3)$$

as long as the ionic abundance does not change significantly between the two components. Meaburn & Walsh (1980) give

$$I_{[\text{Ne v}]}^{\text{wings}} \approx (1/3) I_{[\text{Ne v}]}^{\text{narrow}}. \quad (4)$$

If the ionic abundances were substantially different in the fast wind, such an important contribution to the total line flux would put into question photoionization models. A two-phase nebular gas should be considered. Our IR observations do not show the fast wind, so the photoionization models presented here should not be affected because we use no optical lines. A detailed photoionization model including a range of optical and infrared lines could constrain possible variations in ionic abundances among the two phases. None the less, under the assumption that ionic abundances do not change between clump and fast wind, the range of physical conditions in the fast wind that gives a [Ne v] line ratio of 1/3 is shown in Fig. 13, together with the corresponding ratio for the case of [Ar VI] and [Mg VIII]. The noise levels reported in Fig. 3 yield the following upper limits on the broad wing fluxes in [Mg VIII] and [Ar VI], assuming the broad wing flux is uniformly distributed over 800 km s^{-1} ,

$$I_{[\text{Mg VIII}]}^{\text{wings}} \lesssim 0.02 I_{[\text{Mg VIII}]}^{\text{narrow}} \quad (5)$$

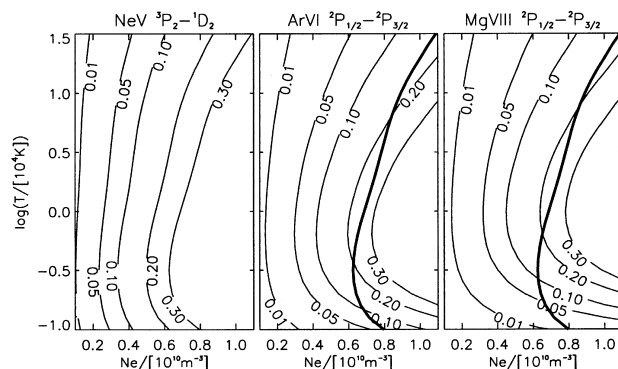


Figure 13. Estimation of the ratio of the broad component to the narrow component as a function of $\log(T/10^4 \text{ K})$ (ordinate) and electron number density. The transitions correspond to [Ne v] 3426 Å and [Ar VI] 4.528 μm , and [Mg VIII] 3.0284 μm . The thick line limits the locus of $\{\log(T/10^4 \text{ K}), N_e\}$ that can account for the broad wings observed in [Ne v] 3426 Å.

$$I_{[\text{Ar VI}]}^{\text{wings}} \lesssim 0.2 I_{[\text{Ar VI}]}^{\text{narrow}} \quad (6)$$

Using Fig. 13, it can be concluded that broad wings should also be apparent in [Ar VI], and especially in [Mg VIII], for the acceptable values of densities and temperatures. It seems that collisional excitation cannot account for the broad wings observed in the optical, at least in these simple terms. A more thorough study including a broader range of lines is required.

5 CONCLUSIONS

The high-excitation PNe NGC 6302 and 6537 have been studied with medium- and high-resolution infrared spectroscopy. We provide a new IR estimate for the heliocentric radial velocity of NGC 6302, finding a $4.1 \pm 2.7 \text{ km s}^{-1}$ difference from optical estimates, possibly owing to extinction within the ionized region. The coronal-line wavelengths that we derive are in agreement with those of Reconditi & Oliva (1993), but not with those of Feuchtgruber et al. (1997).

Our medium-resolution spectra show [Si IX] $3.934 \mu\text{m}$ in emission, which is used with other IR coronal ions to confirm the nebular excitation mechanism to be photoionization, corresponding to a blackbody central star temperature of about 250 000 K for NGC 6302. The only anomalous elemental abundance derived from our NGC 6302 spectra is that of aluminium, found to be depleted relative to solar by a factor of more than 100, presumably owing to being locked in grains. The strong Al depletion implies that some dust is well mixed with the highly ionized gas where the radiation field is hard enough to produce Al VI, at $IP = 154 \text{ eV}$. A similar Al depletion is inferred for NGC 6537. For the case of single star evolution, the revised central star temperature for NGC 6302 is consistent with post-AGB model tracks (Blöcker 1995) for ZAMS masses between 4 and $5 M_{\odot}$. The N/O and C/O gas-phase abundance ratios of NGC 6302 are also consistent with a progenitor main-sequence mass $\lesssim 5 M_{\odot}$, from an adaptation of the synthetic AGB models of Gronewegen & deJong (1993).

Our IR echelle observations reveal that the infrared coronal lines are very narrow and strongly peaked at the centre, with no evidence of broad wings from fast winds. The discrepancy with the $\sim 1000 \text{ km s}^{-1}$ broad wings previously observed for [Ne V] 3426 \AA cannot be explained by collisional excitation in a photoionized gas, at least in a simplified treatment. Further observations are required to confirm the [Ne V] broad wings, and to build detailed models of the interaction between the fast stellar wind and the nebula. The narrowness of the line profiles also makes NGC 6302 and 6537 ideal objects for the study of fine structure in coronal ions. The high-resolution observations show that the cores are stratified in ionization stages, consistent with a photoionized nebula of uniform density. At 8 arcsec offset from the centre of NGC 6302, Bry shows double-peaked profiles, in agreement with previous optical studies based on recombination lines and [N II]. In contrast, the line profiles from the coronal ions are single-peaked at the same offset. Thus, our observations show no signs of a wind-blown bipolar cavity. The nebula, although clumpy enough to accommodate coexisting winds at very different velocities, seems to have a fairly uniform density as close as 1 arcsec to the nucleus. We suggest that the clumpiness of the nebula precludes the formation of a wind-blown cavity.

ACKNOWLEDGMENTS

We are very grateful to Tom Geballe for obtaining the CGS3 spectra, to Gary Ferland for help with CLOUDY, and to Luc Binette, John Dyson, Tom Hartquist and Melvin Hoare for helpful discussions. We are also grateful to PATT for the time allocation on UKIRT, which is operated by the Joint Astronomy Centre on behalf of the Particle Physics and Astronomy Research Council. SC acknowledges support from Fundación Andes and PPARC through a Gemini studentship.

REFERENCES

- Acker A., 1975, *A&A*, 40, 415
 Aller L. H., Ross J. E., O'Mara B. J., Keyes C. D., 1981, *MNRAS*, 197, 95
 Ashley M. C. B., 1990, *Proc. ASA*, 8, 1
 Ashley M. C. B., Hyland A. R., 1988, *ApJ*, 331, 532 (AH88)
 Barlow M. J., 1983, in Flower D. R., ed., *IAU Symp.* 103, *Planetary Nebulae*. Kluwer, Dordrecht, p. 105
 Barral J. F., Cantó J., Meaburn J., Walsh J. R., 1982, *MNRAS*, 199, 817
 Becker S. A., Iben I., 1979, *ApJ*, 232, 831
 Blöcker T., 1995, *A&A*, 299, 755
 Bryce M., Mellema G., Clayton C. A., Meaburn J., Balick B., López J. A., 1996, *A&A*, 307, 253
 Butler K., Zeippen C. J., 1994, *A&ASS*, 108, 1
 Cantó J., 1980, *A&A*, 86, 327
 Clegg R. E. S., Harrington J. P., Barlow M. J., Walsh J. R., 1987, *ApJ*, 314, 551
 Cohen M., Allamandola L., Tielens A.G.G.M., Bregman J., Simpson J. P., Witteborn F. C., Wooden D., Rank D. M., 1986, *ApJ*, 302, 737
 Corradi R. L., Schwarz H. E., 1993, *A&A*, 278, 247
 Cuesta L., Phillips J. P., Mampaso A., 1995, *A&A*, 304, 475
 Duley W. W., Williams D. A., 1981, *MNRAS*, 196, 269
 Durand S., Acker A., Zijlstra A., 1998, *A&AS*, 132, 13
 Edlén B., 1953, *J. Opt. Soc. Am.*, 43, 339
 Elliot K. H., Meaburn J., 1977, *MNRAS*, 181, 499
 Faúndez-Abans M., Maciel W. J., 1987, *A&A*, 183, 324
 Feibelman W. A., Aller L. H., Keyes C. D., Czyzak S. J., 1985, *Proc. Nat. Acad. Sci.*, 82, 2202
 Ferland G. J., 1996, *Hazy*, a brief introduction to Cloudy, University of Kentucky Department of Physics and Astronomy Internal Report (Hazy)
 Feuchtgruber H. et al., 1997, *ApJ*, 487, 962
 Frank A., Mellema G., 1994, *ApJ*, 430, 800
 Frost C. A., Cannon R. C., Lattanzio J. C., Wood P. R., Forestini M., 1998, *A&A*, 332, L17
 Gail H. P., Sedlmayr E., 1998, *Faraday Discuss.*, 109
 Galavís M. E., Mendoza C., Zeippen C. J., 1995, *A&AS*, 111, 347
 Gomez Y., Moran J. M., Rodriguez L. F., Garay G., 1989, *ApJ*, 345, 862
 Gomez Y., Rodriguez L. F., Moran J. M., 1993, *ApJ*, 416, 620
 Greenhouse M. A., Feldman U., Smith H. A., Klapisch M., Bhatia A. K., Bar-Shalom A., 1993, *ApJS*, 88, 23
 Grevesse N., Anders E., 1989, in Waddington C. J., ed., *AIP Conf. Proc.* 183, *Cosmic Abundances of Matter*. AIP, New York, p. 1
 Grevesse N., Noels A., 1993, in Prantzos N., Vangioni-Flam E., Casse M., eds, *Origin and Evolution of the Elements*. Cambridge University Press, Cambridge, p. 15
 Gronewegen M. A. T., deJong T., 1993, *A&A*, 267, 410
 Henry R. B. C., Kwitter K. B., Dufour R. J., 1999, *ApJ*, 517, 782
 Huggins P. J., Healy A. P., 1989, *ApJ*, 346, 201
 Hummer D. G., Storey P. J., 1987, *MNRAS*, 224, 801
 Icke V., Preston H. L., Balick B., 1989, *AJ*, 97, 462
 Icke V., Mellema G., Balick B., Eulderink F., Frank A., 1992, *Nat*, 355, 524
 Johnson C. T., Kingston A. E., Dufton P. L., 1986, *MNRAS*, 220, 155
 Kingdon J. B., Ferland G. J., 1997, *ApJ*, 477, 732

- Kwok S., Purton C. R., FitzGerald P. M., 1978, *ApJ*, 219, L125
 Lame N. J., Ferland G. J., 1991, *ApJ*, 367, 208
 Leg er A., Puget J.-L., 1984, *A&A*, 137, L5
 Leisy P., Dennefeld M., 1996, *A&AS*, 116, 95
 Lennon D. J., Burke V. M., 1994, *A&AS*, 103, 273
 Lester D. F., Dinerstein H. L., 1984, *ApJ*, 281, L67
 Marconi A., van der Werf P. P., Moorwood A. F. M., Oliva E., 1996, *A&A*, 315, 335
 Meaburn J., Walsh J. R., 1980, *MNRAS*, 191, 5
 Mellema G., Frank A., 1997, *MNRAS*, 292, 795
 Milne D. K., Aller L. H., 1975, *ApJ*, 38, 183
 O'Dell C. R., 1998, *AJ*, 116, 1346
 Oliva E., Salvati M., Moorwood A. F. M., Marconi A., 1994, *A&A*, 288, 457
 Oliva E., Pasquali A., Reconditi M., 1996, *A&A*, 305, L21
 Osterbrock D. E., 1989, *Astrophysics of Gaseous Nebulae and Active Galactic Nuclei*. W. H. Freeman and Company, San Francisco
 Outred M., 1978, *J. Phys. Chem. Ref. Data*, 7, 1
 Payne H. E., Phillips J. A., Terzian Y., 1988, *ApJ*, 326, 368
 Pelan J., Berrington K. A., 1995, *A&AS*, 110, 209
 Pottasch S. R., Beintema D., 1997, *ESA SP-419, Proc. First ISO Workshop on Analytical Spectroscopy*. ESA Publications, Noordwijk, p. 118
 Pottasch S. R., Beintema D., Dominguez-Rodr guez F. J., Schaeidt S., Valentijn E., Vandenbussche B., 1996, *A&A*, 315, L261
 Pwa T. H., Mo J. E., Pottasch S. R., 1984, *A&A*, 139, L1
 Pwa T. H., Pottasch S. R., Mo J. E., 1986, *A&A*, 164, 184
 Reconditi M., Oliva E., 1993, *A&A*, 274, 662
 Renzini A., Voli M., 1981, *A&A*, 94, 175
 Rieke G. H., Lebofsky M. J., 1985, *ApJ*, 288, 618
 Roche P. F., 1989, in *Torres Peimbert S., ed., IAU Symp. 131, Planetary Nebulae*. Kluwer, Dordrecht, p. 117
 Roche P. F., Aitken D. K., 1986, *MNRAS*, 221, 63
 Rodr guez L. F. et al., 1985, *MNRAS*, 215, 353
 Rothman L. S. et al., 1992, *J. Quant. Spectrosc. Radiat. Transfer*, 48, 469
 Rowlands N., Houck J. R., Herter T., 1994, *ApJ*, 427, 867 (RHH)
 Saraph H. E., Storey P. J., 1996, *A&AS*, 115, 151
 Saraph H. E., Tully J. A., 1994, *A&AS*, 107, 29
 Shields G. A., 1983, in *Flower D. R., ed., IAU Symp. 103, Planetary Nebulae*. Kluwer, Dordrecht, p. 259
 Smits D. P., 1991, *MNRAS*, 251, 316
 Waters L. B. F. M., Molster F. J., de Jong T. et al., 1996, *A&A*, 315, L361
 Weaver J., McCray R., Castor J., Shapiro P., Moore R., 1977, *ApJ*, 218, 377
 Wilson O. C., 1950, *ApJ*, 111, 279
 Zhang H. L., Graziani M., Pradhan A. K., 1994, *A&A*, 283, 319
 Zhekov S. A., Perinotto M., 1996, *A&A*, 309, 648

APPENDIX A: FLUXES AND ACCURATE WAVELENGTHS FOR FINE-STRUCTURE LINES, AND THE HELIOCENTRIC VELOCITIES OF NGC 6302 AND 6537

A number of fine-structure lines can be found in the spectrum of NGC 6302 and 6537, of which the accurate wavelengths represent valuable information and can be compared with previous measurements. The low-resolution spectra were calibrated using nebular H I lines when present near the lines of interest, otherwise using a quadratic fit to Ar or Kr arc lamp spectra (deviations from a linear law were found to be negligible). The calibration of the echelle observations is described below. We found the heliocentric velocity of NGC 6302 to be $-34.8 \pm 1 \text{ km s}^{-1}$, using H I 5–10 at $3.0384 \mu\text{m}$ in the two [Mg VIII] frames. This corresponds to $-27.3 \pm 1 \text{ km s}^{-1}$ in the local standard of rest (kinematic LSR), which agrees closely with the H76 α measurement of $-29 \pm 2 \text{ km s}^{-1}$ by Rodr guez et al. (1985, their fig. 2 shows that the

observed peak is redshifted with respect to their Gaussian fit by about 5 km s^{-1}). But the heliocentric velocity of NGC 6302 obtained from optical studies (compilation by Durand et al. 1998, based on Acker 1975) has been reported to be $-38.9 \pm 2.5 \text{ km s}^{-1}$. On the other hand, we measure a heliocentric velocity for NGC 6537 of $-17.8 \pm 3 \text{ km s}^{-1}$, using H I 5–11 at $2.872213 \mu\text{m}$ on the [Al IV] frame, which is in agreement with the value listed in Durand et al. (1998) of $-16.9 \pm 1.9 \text{ km s}^{-1}$. It should be stressed that the long wavelength side of H I 5–11 was very noisy, the heliocentric velocity we report for NGC 6537 assumes that the width of the line is the same as for Br γ , but any error would result in a higher (i.e. redshifted) velocity.

By adopting the estimated systemic velocities from the echelle spectra, we can achieve consistent wavelength determinations for the extinction insensitive infrared coronal lines. Considering the quoted uncertainties in the case of NGC 6302, there could be a slight discrepancy with the optical measurements, which is most likely due to internal extinction within the ionized regions of the nebula. Huggins & Healy (1989) report a CO(2–1) centroid for NGC 6302 of $V_{\text{lsr}} = -40 \text{ km s}^{-1}$, blueshifted in excess of 10 km s^{-1} from the measurements reported here. The CO(2–1) profile is double-peaked, and the approaching side has about twice the peak brightness temperature as the receding side (we conducted SEST observations of $^{13}\text{CO}(2-1)$ which show the same profile, and that shall be presented in a forthcoming article), hinting at possible radiative-transfer effects. However, we do not base any of the following on the mm-line centroids, because the line of sight towards NGC 6302 crosses cold galactic molecular emission.

Table A1 gives a summary of our measurements, where wavelengths are given in air and in the nebular rest frames (the refractive index of standard air as a function of wavelength was taken from Edl n 1953). The uncertainty in the calculated wavelengths is dominated by the accuracy of the adopted heliocentric velocities, in the best cases. Below we provide some notes and compare our measurements with those found in the literature, where available.

[Mg VIII]: we have two echelle measurements corresponding to the two slit orientations. A comparison of the standard star spectra with a high-resolution atmospheric transmission model (based on the HITRAN data base, Rothman et al. 1992) gave an initial quadratic fit to the dispersion law, which we used to identify Argon lines from the arc-lamp frames. The arc-lamp calibration agrees very well with the atmosphere calibration, although with shifts of the order of 10 km s^{-1} towards the edges of the array, which probably stem from the standard star not being precisely centred within the 1-arcsec slit. We used the arc lamp to calibrate the [Mg VIII] frame. Many lines were identified as leaks from neighbouring orders, i.e. the Argon arc-lamp spectra in order 36 also showed lines from orders 37 and 38, implying that the CVF blocked wavelengths outside of about $0.1 \mu\text{m}$ from the CVF wavelength of $1.515 \mu\text{m}$. The calibrated dispersion axis is strongly non-linear, with deviations from a linear law of up to 20 km s^{-1} , and offset from the estimated scale by -300 km s^{-1} to -50 km s^{-1} from side to side of the array. We estimate the uncertainty in the [Mg VIII] wavelength to be 2 km s^{-1} , dominated by the relative velocity of NGC 6302. H I 5–10 is on the same frame, and allows an accurate estimate of the Doppler shift from NGC 6302. The low-resolution spectrum estimate is accurate to better than one sample element (i.e. $R = 1500 \times 3$), but the secondary line is blended.

[Ar VI]: the echelle wavelength calibration was based on a

Table A1. Rest wavelengths (in air) for emission lines from NGC 6302, or from NGC 6537 when specified. The numbers in brackets are the uncertainties in the last decimal places. Fluxes are given for the whole slit, without correction for extinction or blends and with a typical uncertainty of 20 per cent. The slit orientation for each line can be inferred from the tabulated fluxes.

| Ion | $i < j$ | λ [μm] | | λ [μm] ^b | | Flux [W m^{-2}] | | |
|-----------------------|-------------------------------------|-----------------------------|---------------|--|---------------------------|----------------------------|-----------------------|-----------------------|
| | | $R = 1500$ | $R = 20\,000$ | (reference) | \parallel 3-arcsec slit | \parallel 1-arcsec slit | \perp 1-arcsec slit | |
| Si VI | $^2\text{P}_{3/2}-^2\text{P}_{1/2}$ | | 1.96287(10) | 1.96287(10) | (3) | | 1.6×10^{-16} | |
| Si VI ^c | $^2\text{P}_{3/2}-^2\text{P}_{1/2}$ | | 1.96311(20) | 1.96287(10) | (3) | | 1.0×10^{-17} | |
| Al V ^c | $^2\text{P}_{3/2}-^2\text{P}_{1/2}$ | | 2.882975(19) | 2.90440(37) | (1) | | 9.6×10^{-18} | |
| Mg VIII | $^2\text{P}_{1/2}-^2\text{P}_{3/2}$ | 3.02788(67) | 3.027661(20) | 3.02713(25) | (3) | 2.9×10^{-15} | 1.7×10^{-15} | |
| (second) ^a | | | 3.027033(20) | | | | 1.9×10^{-16} | |
| Mg VIII | $^2\text{P}_{1/2}-^2\text{P}_{3/2}$ | | 3.027648(20) | 3.02713(25) | (3) | | | 1.4×10^{-15} |
| (second) ^a | | | 3.027003(20) | | | | | 7.3×10^{-17} |
| K VII | $^2\text{P}_{1/2}-^2\text{P}_{3/2}$ | 3.1899(21) | | 3.18966(15) | (1) | 4.2×10^{-16} | | |
| Al VI | $^3\text{P}_2-^3\text{P}_1$ | 3.65952(81) | | 3.661(14) | (2) | 2.1×10^{-16} | | |
| Si IX | $^3\text{P}_0-^3\text{P}_1$ | 3.9346(26) | | 3.935 | (4) | 3.5×10^{-17} | | |
| Ar VI | $^2\text{P}_{1/2}-^2\text{P}_{3/2}$ | 4.5265(30) | 4.52799(15) | 4.52829(31) | (1) | 8.7×10^{-14} | | 2.5×10^{-14} |
| Na VII | $^2\text{P}_{1/2}-^2\text{P}_{3/2}$ | 4.6908(31) | | 4.68344(33) | (1) | 7.4×10^{-15} | | |

^a Unidentified secondary line in the [Mg VIII] 3.028 μm frame.^b Previous measurements from 1, Feuchtgruber et al. (1997, corrected to values in air); 2, Greenhouse et al. (1993); 3, Reconditi & Oliva (1993); 4, Oliva et al. (1994).^c Measured from NGC 6537.

xenon lamp, which showed one arc line only, at 2.261 828 3 μm (Outred 1978) in second order, very close to the centre of the array. Because of the modulation owing to the CVF fringes it was impossible to use the standard star spectrum to calibrate the wavelength dispersion. We used the quadratic dispersion law for [Mg VIII] 3.03 μm , shifted to match the xenon arc line. The uncertainty should be about 10 km s^{-1} . The low-resolution spectrum did not provide a satisfactory measurement because the line was strongly affected by random bad pixels, with an accuracy of about one resolution element.

[Al V]: here the echelle spectrum was of NGC 6537, rather than NGC 6302. We calibrated the dispersion axis by the same procedure as for [Mg VIII], and confirm that the CVF does not block wavelengths within 0.1 μm from the CVF wavelength. H I 5–11 2.872 213 μm was also present in the same frame. Although it is noisy, this line allows an estimate of the systemic velocity of NGC 6537. No measurements are provided for the low-resolution spectrum because the line is blended with H I 5–11, which represents about 75 per cent of the flux.

[Si VI]: we used the airglow OH line at 1.958 78 μm (1.95932 μm in vacuum from the UKIRT worldwide webpages). The line is very faint and was discernible across the array only after co-adding all the object frames, and there is an uncertainty of about 10 km s^{-1} in the position of the line. The standard star spectra seem to be affected by local absorption related to the instrument, which is also apparent in the nebular continuum emission from both PNe. The solar spectrum is at odds with the standard star spectra, so unfortunately the atmosphere cannot be used for calibration. We adopted the dispersion scale from the [Mg VIII] frame shifted to match the OH line. An uncertainty of no less than 10 km s^{-1} is expected in the dispersion scale, and the [Si VI] wavelength is thus accurate to about 15 km s^{-1} .

[Al VI]: only a low-resolution wavelength determination is available, but it should be reliable because that spectrum showed many other lines, which all match the reference wavelengths. However, the best accuracy achievable is probably not better than one sample element, or 67 km s^{-1} ($R = 1500$ oversampled 3 times), because the line is noisy and lies near a zone of strong atmospheric absorption.

[Si IX]: this line was calibrated using nearby H I Hu15, but it is faint and the accuracy is only one resolution element. The

Table A2. Fluxes of emission lines in the 8–13 μm spectra of NGC 6302 and 6537 (in $10^{-14} \text{ W m}^{-2}$), and comparison with *ISO* measurements.

| | <i>IP</i> [eV] | NGC 6302 | | NGC 6537 |
|-----------------------------|-------------------|----------|-------------------|----------|
| | | CGS3 | <i>ISO</i> | CGS3 |
| [Ne VI] 7.64 μm | 126.1 | 81.9 | 63.0 | 13.5 |
| [Ar V] 7.90 μm | 59.8 | 1.18 | – | 0.86 |
| [Na VI] 8.62 μm | 138.4 | 0.56 | 1.1 | 0.23 |
| [Ar III] 8.99 μm | 27.6 | 1.76 | – | 0.80 |
| [S IV] 10.5 μm | 34.8 | 4.77 | 8.5 ^a | 6.77 |
| [Ne II] 12.8 μm | 21.6 | 3.23 | 14.7 ^a | 1.14 |
| [Ar V] 13.1 μm | 59.8 | 0.56 | 2.9 | 0.61 |

^a From Pottasch & Beintema (1997), the other *ISO* fluxes are from Pottasch et al. (1996).

resulting wavelength is in good agreement with the measurement from the coronal spectrum of the Circinus galaxy by Oliva et al. (1994). This comes as a confirmation for their adopted radial velocity because in Circinus the narrow line region is blueshifted relative to the systemic velocity, and [Si IX] is about 300 km s^{-1} broad.

Finally, [K VII] was calibrated with respect to an Argon arc lamp and [Na VII] with respect to the nearby He II 6–7 line, although both were quite noisy and so the wavelengths are estimated to be accurate to only one resolution element.

The low-resolution and the echelle measurements are consistent, and agree in general with other published results, except for the *ISO* measurements of Feuchtgruber et al. (1997). The agreement with Reconditi & Oliva (1993) is improved when using the optical heliocentric velocity of NGC 6302 discussed above.

The fluxes for emission lines in the CGS3 spectra are listed in Table A2, together with the *ISO* fluxes from Pottasch & Beintema (1997) and Pottasch et al. (1996). In order to compare the CGS3 and *ISO* fluxes, correction factors need to be applied to account for the different beam sizes, which can be estimated using the spatial information from the low-resolution CGS4 spectra. In the case of NGC 6302, at a 3-arcsec pixel size, the average spatial full width at half-maximum (FWHM) of H I lines along the slit was 2.8 pixels, and all coronal ions had approximately the same width

of 2 pixels. For NGC 6537, the H I FWHM was 1.7 pixels, and the coronal ions covered approximately 1.3 pixels along the slit. These results suggest that, for the purpose of scaling fluxes to the central 3 arcsec, all ions can be approximated to have the same spatial extent. At the higher spatial resolution of the echelle observations (see Fig. 11) the FWHM for [Mg VIII], [Si VI] and [Ar VI] are about 3, 4 and 5 arcsec, and ions with ionization potentials ~ 100 eV would have a spatial extent between Si VI and Ar VI. The fluxes from large beam observations should thus be about 2–3 times higher than from the central 3 arcsec. This seems reasonable for [Mg VIII] $3.028 \mu\text{m}$, listed in Table A1, for which Pottasch et al. (1996) give a flux of $3\text{--}6 \times 10^{-15} \text{ W m}^{-2}$. For NGC 6302, fluxes

through the circular 4-arcsec aperture of CGS3 should thus be 2–3 times less than the fluxes for the whole nebula, assuming the emission lines have uniform surface brightness over the central square 5–6 arcsec. From Table A2, a correction factor of ~ 2.5 matches [Na VI] $8.62 \mu\text{m}$ and [S IV] $10.52 \mu\text{m}$. We attribute the larger correction factor required for [Ne II] $12.8 \mu\text{m}$ to a larger spatial extent, but the [Ne VI] $7.64 \mu\text{m}$ fluxes are discrepant. [Ne VI] lies on the edge of the atmospheric window, and is likely to be affected by unresolved atmospheric transmission features.

This paper has been typeset from a $\text{\TeX}/\text{\LaTeX}$ file prepared by the author.